Graphene/Ionic Liquid Ultracapacitors: Does Ionic Size Correlate with Storage Energy Performance?

Vitaly V. Chaban,[1] Nadezhda A. Andreeva,[2] and Eudes Eterno Fileti [3*]

(1) P.E.S., Vasilievsky Island, Saint Petersburg, Leningrad oblast, Russian Federation.
(2) Department of Physics, St. Petersburg State University, 198504, St. Petersburg, Russian Federation.
(3) Instituto de Ciência e Tecnologia, Universidade Federal de São Paulo, 12247-014, São José dos Campos, SP, Brazil.

Abstract. An electric double layer ultracapacitor stores energy in an electric double layer formed near its electrolyte/electrode interfaces. Graphene-based ultracapacitors, because of their outstanding performance, have attracted significant research interest. Optimization of ultracapacitor performance requires understanding the correlation of molecular characteristic of the device (such as structure, inter-ionic and ion-electrode interactions) with its macroscopic properties. Herein, we report molecular dynamics study of how an ionic volume impacts a double-layer capacitance. Four systems were probed: large cation + large anion, large cation + small anion, small cation + large anion; small cation + small anion. Our results show that the structuring of the ionic liquid is driven by the electrolyte-electrode interactions in the ultracapacitor, which are predominantly of the van der Waals type. Storage density energies are similar for all ultracapacitors, being in the range of 24 to 28 J cm^{-3} at 5.0V. Our results present a comparative analysis of the performances of four different ILs confined between two graphene electrodes. Although the best performance has been observed for the IL with ions (cations and anions) of equal sizes, no definite conclusion about the correlation of the performance to the ionic size ratio can be made from the present study.

Introduction

An ultra(super)capacitor has attracted significant attention, mainly due to their high power density, low internal resistance, high charge/discharge rates, and long life cycle performance.[1-4] Ultracapacitors consist of two electrodes, an electrolyte and a separator that electrically isolates the two electrodes and their performance inherently depends on the electrical nature of these two components.[1-4] Optimizing the performance of an ultracapacitor consists of maximizing its energy density, which can be achieved by increasing its capacitance and voltage and at the same time reducing its internal resistance. As such properties depend on the materials used in the device design, the development of a high performance ultracapacitor will depend on the development of new materials to be used as electrodes and electrolytes.[3] The requirements for an electrolyte in a ultracapacitor include: high electrochemical stability, high ionic concentration and smaller solvation radius, low electric resistivity, low viscosity, low volatility, low environmental toxicity. Therefore, ionic liquids have been considered as natural candidates.[5-8]

As the chemical–physical properties, in special the conductivity, of ionic liquids strongly depend on the type and size of cation and anion, it is to be expected that the properties of an ionic liquid-based ultracapacitor also depends on the size of the ions constituting the ionic liquid employed in the device. Although there are many recently published works where ionic liquids of different classes are considered as electrolytes in ultracapacitors,[5] a direct comparison of the effect of each type of liquid becomes complex due to the different characteristic parameters of the devices investigated in each of the works, such as surface charge density, geometry, types of electrodes, electrolyte concentration, etc. Among the most recent studies,

many have devoted themselves to the study of parallel plate ultracapacitors using ionic liquids in order to rationalize the influence of ion size and type on ultracapacitor performance.[9-11] For example, Wu and co-workers investigated the performance of four different amino acid ionic liquids as electrolytes in ultracapacitors varying the size of the anions for the same cation. They found that the C-V curve was shown independent of the size of the anions and that this invariance was due to the geometrically heterogeneous distribution of anion charges mainly located in the carboxylate group.[9] Vatamanu et al., determined the dependence of capacitance with cation size (for a fixed anion) for four different graphite ultracapacitor using electrolytes Cnmim-TFSI (with n = 2, 4, 6, and 8) as electrolytes.[10] The results indicated that the increase of the alkyl tail length of the cation resulted only in a small reduction in DC, indicating ions ability to rearrange/reorient charge carrying groups such that it maximizes the counterions charge near the surface of the electrode. The same group, in a study on porous electrodes, indicates that the size of the ions is an important parameter to be varied to optimize the energy storage of EDL capacitors.[11] In the specific case of the interaction of the electrolyte with a nanopore, the size and shape of the cations and anions can be used for such optimization.[11]

In this work, we investigate the performance of ultracapacitors with four different ionic liquids as electrolytes by means of atomic simulations of molecular dynamics. The results obtained for the four ultracapacitors are directly comparable since the dimensions of the ultracapacitors essentially the same. In addition, the employed ionic liquids are based on two different types of cations and two different types of anions, so that we can examine the influence of the shape, size and nature of the ionic liquids by the thickness of the electric double layer and the capacitance. This will allow us to quantify the contributions of each type of ions to ultracapacitor properties.

Computational details

The ultracapacitors considered here consist of an ionic liquid (electrolyte) confined between two planar and rigid graphene sheets (electrodes). We prepare four ultracapacitors with four different electrolytes: N-butyl-N-methylpyrrolidinium bis(trifluoromethylsulfonyl)imide (PYR-TFSI), N-butyl-N-methylpyrrolidinium hexafluorophosphate (PYR-PF6), butyltrimethylammonium bis(trifluoromethylsulfonyl)imide (BMA-TFSI) and butyltrimethylammonium hexafluorophosphate (BMA-PF6). The choice of these ions was determined by their size and shape. It was assumed that the size of the cation BMA and anion PF6 are smaller and more compact than the cation PYR and anion TFSI. In fact this can be confirmed by their molar masses: M(BMA)=116.2 g mol^{-1}, M(PF6)=145.0 g mol^{-1}, M(PYR)=142.3 g mol^{-1}, M(TFSI)=280.2 g mol^{-1}. The systems and their basic properties are given in Table 1.

Table 1: Composition of the investigated systems.. The number of ionic pairs in each ultracapacitor was adjusted to provide the same value for the distance between the electrodes. This adjustment also led to bulk density equal to that for the corresponding pure liquid, thus the X (3.44 nm), Y (3.40 nm) and Z dimensions are the same (13 nm) for all supercapacitors.

System	# ion pairs	# interaction sites
PYR-TFSI	264	12776
PYR-PF6	333	13217
BMA-TFSI	282	12458
BMA-PF6	360	12776

The cross section of each computational cell was determined by the dimensions of the graphene electrodes: 3.44x3.40 nm^2, which are separated by a distance d = 13 nm shown in Table 1. The number of ion pairs in each ultracapacitor was adjusted to provide the same inter-electrode distance for all systems as well as to achieve a bulk density equal to that of pure liquids. A slab of 30 nm of vacuum was left outside the confining sheets for avoiding artificial influence from periodic images. Periodic boundary condition or minimum image convention has been applied in all of the x, y and z-directions. Spatial structures of ions constituting the ionic liquids and a molecular representation of the ultracapacitor are shown in Figure 1.

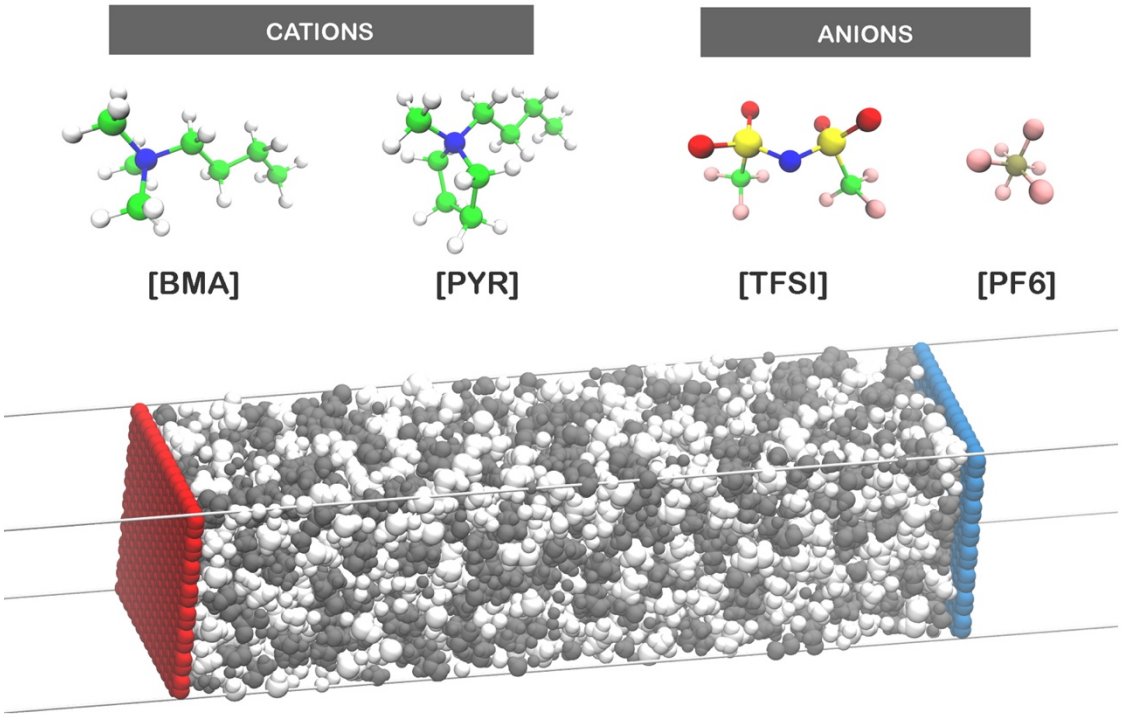

Figure 1: (Top) Spatial structures of ions constituting the investigated electrolytes. Hydrogen atoms are white, carbon atoms are green, nitrogen atoms are blue, oxygen atoms are red, sulfur atoms are yellow, fluorine atoms are pink and phosphorus atom is brown. (Bottom) Ultracapacitor model composed of two graphene monolayers and [BMA][TFSI] as an electrolyte. The right electrode is positively charged (in blue), the left electrode is negatively charged (in red).

From the pre-relaxed cells at constant pressure, MD simulations were performed in the isothermal-isochoric ensemble (N,V,T). We simulated the systems with PYR-TFSI, PYR-PF6 or BMA-TFSI as electrolyte at a 500 K. The system with BMA-PF6 was simulated at a higher temperature, 600 K, because at this temperature the system remains liquid, thus avoiding crystallization of the system. A solvent should be used for the system BMA-PF6 at lower temperatures. Additionally, high temperature allows to accelerate the dynamics and avoid multiple metastable states, which are abundant in many ionic liquids at room temperature. Constant temperature was maintained by the velocity rescaling thermostat with a relaxation time of 500 fs.[12]

Graphene electrodes were simulated as a non-polarizable assembly of carbon atoms fixed in its hexagonal lattice with distance (C-C) = 1.41 nm.[13, 14] The Lennard-Jones (12,6)

parameters for the sp^2 carbon were taken as follows: σ=0.34 nm, ε=0.36 kJ mol^{-1}.[13, 14] The ionic liquids were simulated using the force field introduced by Chaban et. al.[15-17] This model provides correct thermodynamic and transport properties in a wide temperature range.

The ultracapacitors were simulated at 11 different surface charge densities on the electrodes from $\sigma_s = 0$ (discharged ultracapacitor) to $\sigma_s = \pm 1.0\ e\ nm^{-2}$ ($\sigma_s = \pm 16\ \mu C\ cm^{-2}$) equally incremented by $0.1\ e\ nm^{-2}$ ($1.6\ \mu C\ cm^{-2}$). These densities correspond to a voltage range that is greater than the electrochemical window of an ionic liquid-based electrolyte. It is worth to note that ionic liquids withstand a finite voltage around 5V,[5] so very high charge densities can lead to physically unacceptable models. From an computational modeling point of view the extrapolation of this limit is justified the light of analyzes and inferences that can be performed. In addition, this surface charge density range is a typical surface charge density and has already been employed in recent work involving graphene-based ultracapacitors.[18-21] All systems were pre-equilibrated during 5.0 ns. Equilibrium properties were determined from the 20 ns long production runs. The integration time-step of 1.0 fs was used. The long-ranged electrostatic interactions were simulated by an parallelized subroutine implementing the Particle-Ewald-Mesh method.[71] The Lennard-Jones (12,6) potential was modified in the range 1.1-1.2 nm by the switch method for the corresponding interaction to exactly vanish at the cut-off distance between the interacting atoms. Coordinates and intermediate thermodynamic quantities were saved every 200 fs. All reported MD simulations were performed using the GROMACS 2016 molecular simulation engine.[22, 23]

Results

Pure liquids

Tables 2 summarizes physical properties (density, heat of vaporization, diffusion) for all of ionic liquids used as electrolytes in this work. The density value is governed by the characteristics of the anion, being about 1350 kg m^{-3} for TFSI based liquids about 1175 kg m^{-3} for PF6 based liquids. The vaporization enthalpy does not show any tendency in relation to the volume of the ion pairs, with the liquid BMA-PF6 having the highest value for enthalpy while BMA-TFSI has the lowest value.

The diffusion coefficients indicate that in the liquids with the largest anion, the cation is more mobile than the anion. For example, for liquid PYR-TFSI the diffusion constant for the cation, D(+), is 6.2 $\mu m^2 s^{-1}$ while that of the anion, D(-), is 4.6 $\mu m^2 s^{-1}$. On the other hand, for the liquid with the smaller anion, the mobility of the cation is virtually the same of the anion. Thus, it is expected that TFSI-based electrolytes will exhibit conducting properties different from those based on PF6.

Table 2: Mass density, heat of vaporization and diffusion coefficients obtained from bulk simulations. Errors in D are the standard deviation.

System	ρ (kg m^{-3})	ΔH_{vap} (kJ mol^{-1})	D(+) ($\mu m^2 s^{-1}$)	D(–) ($\mu m^2 s^{-1}$)
PYR-TFSI	1341 [1381[a]]	156[152[b]]	6.2±0.6[10.8±5[a]]	4.6±0.7[9±5[a]]
PYR-PF6	1171	154	2.4±0.5	2.4±0.7
BMA-TFSI	1356 [1369[c]]	138	5.4±0.2	4.8±0.4
BMA-PF6	1179	162	2.3±0.8	2.4±1.2

a) Ref. [24]. b) Ref. [25]. c) Ref. [26]. All experimental data are for low temperatures, 293 to 353K.

Structure and energetics of the supercapacitors

The interfacial properties of electric double layer for ionic liquids near electrified surfaces can be characterized by number density profiles as a function of separation from the electrode surface. Figure 2 presents the number density profiles for the electrolyte PYR-TFSI near to charged electrodes. It is clearly shown that the electrode surfaces, that are characterized by negative and positive charges, lead to distinct stacking behavior of absorbed ILs on these

two surfaces, as observed in previous works.[9-11, 27-29] For example, for the distribution of TFSI anions near the surface of the positive electrode (red areas from Figure 2), we observed an approximately linear increase in height of the first peak with charge density, from 60 to 85 nm^{-3}. For higher density, beyond $0.8\ e\ nm^{-2}$, the first peak divides in two because of the strong structuring of TFSI anions which consisting of two separate equivalent groups (see Figure 1). The same distribution (not shown), but on the negative surface, has peaks with much lower heights (in average 40 nm^{-3}) as a consequence of strong Coulomb repulsion between anion and negative electrode. For all charge densities, the structuring effects are seen up to about 2.5 nm from the surface of the electrodes, distance beyond which the electrolyte presents bulk density.

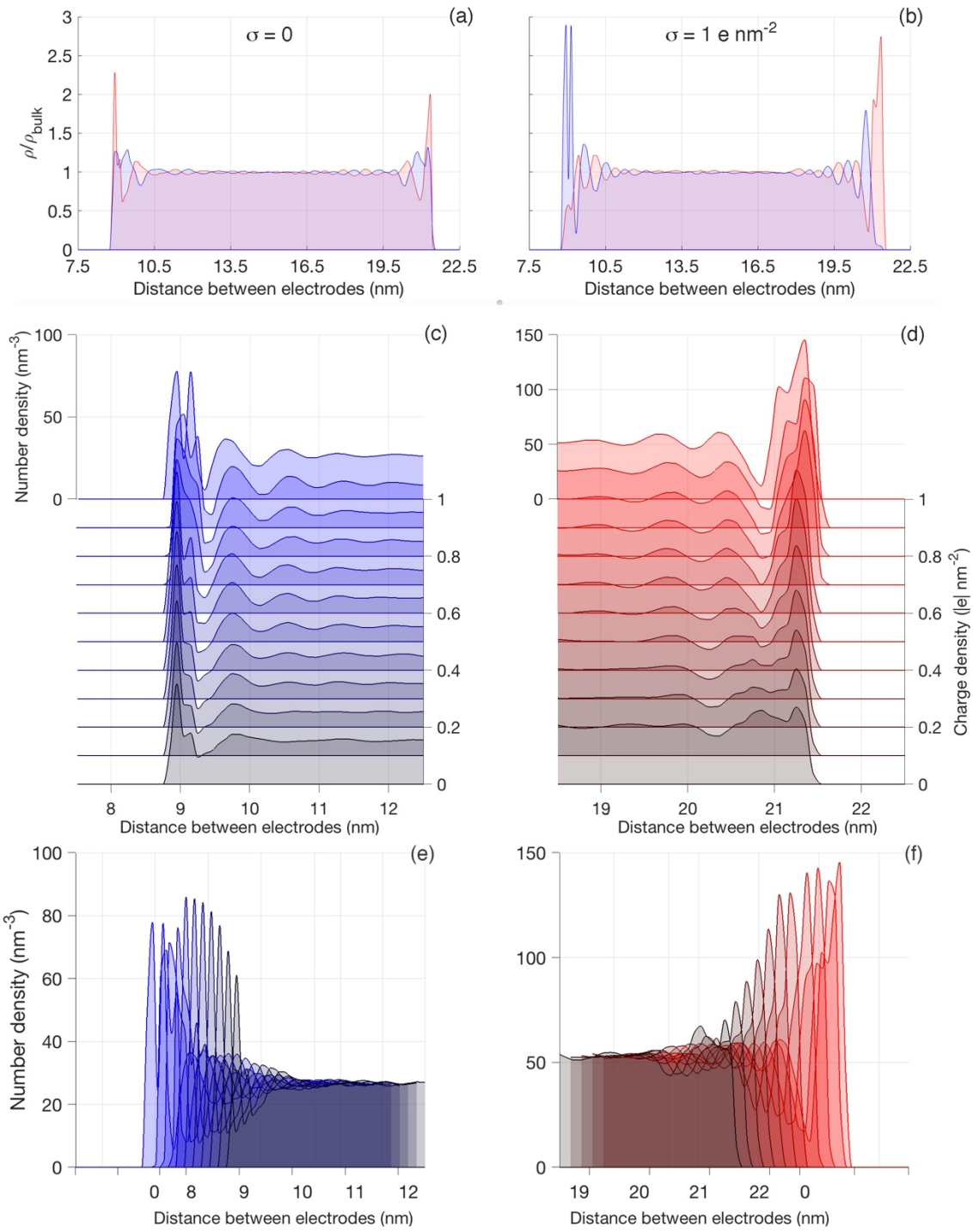

Figure 2. At top, the superposition of the normalized distributions for the anions and cations for both uncharged (a) and charged (b) electrodes. At middle, show the density (unnormalized) of anions near positive electrode (blue area, (c)) and cations near negative electrode (red area, (d)) near the charged electrodes. At bottom, (e) and (f), are the same from (c) and (d) but with a slightly rotated perspective to facilitate comparison between profile peaks. These results correspond to the liquid PYR-TFSI; for the other electrolytes the profiles are similar and presented in the supporting material.

The oscillatory character of the number density profiles usually varies with σ and d (distance between the electrodes).[9-11, 27-29] Cation and anion structures in general oscillate in

phase, ie, their peak positions along z generally coincide. Additionally, as expected, the structures of anions and cations near the charged electrode become, respectively, enhanced and reduced, compared to those near the uncharged electrode. This behavior can be observed at the density profiles for the all electrolytes obey similar standards and are presented in the supporting material. For instance, in the case of uncharged electrode, the ion density distribution reaches a maximum at a distance of 0.6 to 0.9 nm from the electrode surface for all ultracapacitors. To examine this, we performed a direct comparison between the distributions of the anions and cations for the four liquids in the uncharged supercapacitors. From that we determined the exact value of the distance from the first peak to the electrode plane (at z = 8.55 nm or z = 21.5 nm). With this we verified that the distances are in the range of 0.6 to 0.9 nm for the anions and 0.5 to 0.8 for the cations, as showed at Figure S2. This increase in density of the electrolytes at the graphene interface has been repeatedly described in previous studies in the simulation of atomic and molecular systems.[9-11, 27-29] In the case of the charged electrodes we can observe a redistribution of ion density. The density of cations increases near cathode while the density of anions increases near anode. The thickness of the induced electric double layer is 0.5-0.6 nm for all ultracapacitors.

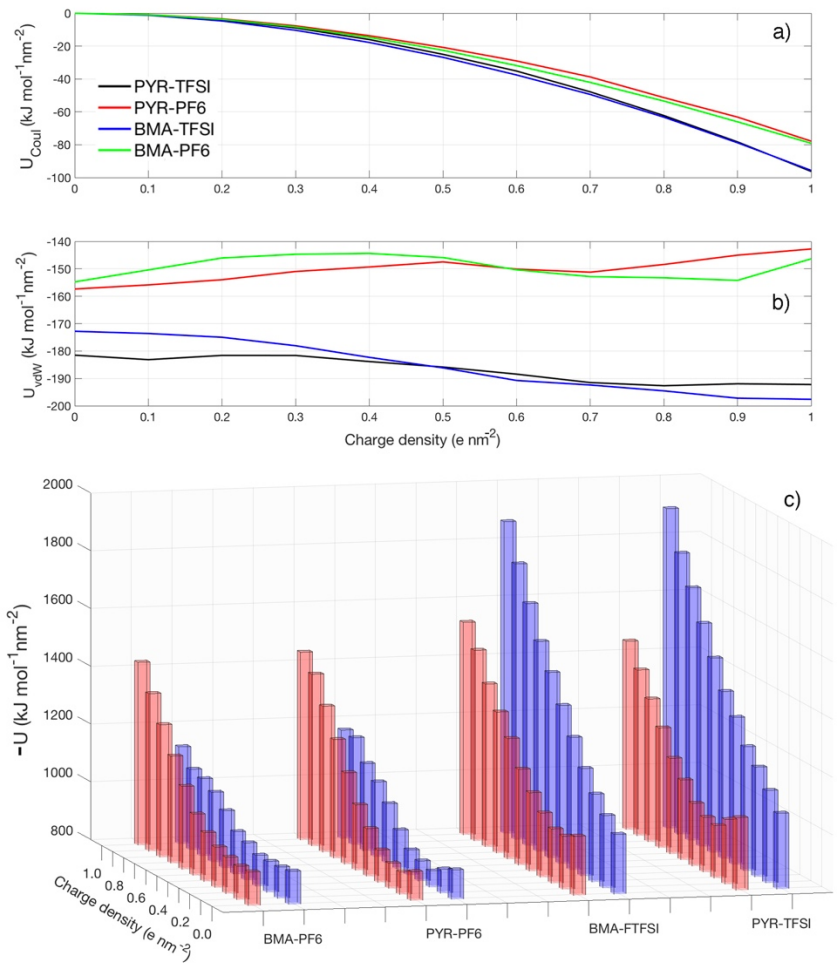

Figure 3: Electrode-electrolyte interaction energies (kJ mol^{-1} nm^{-2}). a) and b) show the Coulomb and van der Waals contributions of the interaction energy between the electrolyte and both electrodes. c) Red and blue bars represent interaction total energy (Coul + vdW) of the electrolytes with negative and positive electrodes, respectively. The energies are normalized with respect to the electrode area. Values in panel c) were multiplied by -1 for the sake of clarity.

The structuring of the electrolyte on the electrode surfaces is closely related to the electrode-electrolyte interaction energy. A strict thermodynamic description of this interaction should also take into account not only the enthalpy contribution but also the entropic one related to the ion rearrangement at the electrified surfaces. However, important information can be obtained considering only the energetic aspect. The decomposition of the total interaction energy between electrolyte and both electrode is shown in Figure 3, where panels 3a and 3b respectively show the Coulomb and van der Waals components, normalized by the area of the electrodes. We can see that the electrostatic components grow quadratically with the charge density, being naturally zero for $\sigma = 0$. The maximum value for this contribution reaches -96

kJ mol^{-1} nm^{-2} for the TFSI-based electrolytes. The contribution of van der Waals, on the other hand, shows little variation in the range of charge densities used. However, it is possible to observe that TFSI-based liquids also have the highest average value for this contribution, -185 kJ mol^{-1} nm^{-2}. This result is expected since the TFSI anion is significantly larger than the PF6. The comparison between the two components shows that from the energy point of view the electrolyte-electrode interaction is largely dominated by the van der Waals interactions.

Figure 3c shows the interaction energy between each of the electrolytes with both electrodes separately. As expected this energy grows monotonically with the charge density for all electrolytes. We also observe that all ionic liquids interact approximately with the same energy with the negative electrode (red bars), ~125 kJ mol^{-1} nm^{-2}. However, for the positive electrode such interaction is quite different. We observed that for the TFSI anion-based liquids the interaction with the positive electrode is ~165 kJ mol^{-1} nm^{-2} whereas for the anion PF6 the same interaction is only 100 kJ mol^{-1} nm^{-2}. This difference is related to the van der Waals contributions from each ion type. For example, it was observed that the electrostatic contributions of the interaction with both electrodes are similar for all ions, with a value between -440 and -520 kJ mol-1 (at σ = 1 e nm^{-2}, see Table S5). On the other hand, the contribution of van der Waals to the interaction with the positive electrode is about twice as large for TFSI as for PF6, which leads to a lower total interaction energy with the positive electrode for the PF6 based ionc liquids, as evidenced in Figure 3c.

Electrical properties and stored energy

The capacitance (C) of the ultracapacitor depends on the surface charge density at the electrode (σ_s) and the drop potential across the device, ($\Delta\Phi = \Phi^{cathode} - \Phi^{anode}$). The surface charge density is taken as the average total charge on the electrode divided by the surface of an electrode, while the drop potential is considered the difference between the electrostatic drop potential in the charged capacitors and their corresponding value in the

capacitors discharged, ($\Delta\Delta\Phi = \Delta\Phi^{charg} - \Delta\Phi^{uncharg}$). In this context, the capacitance of an ultracapacitor can be obtained in two different ways: by the ratio between the charge density and the drop potential, $C_I = {|\sigma_s|}/{\Delta\Delta\Phi}$, (integral capacitance) or by the rate of change of the charge density as a function of the drop potential on a given electrode, $C_d = d\sigma/d\Phi$ (differential capacitance).

The electrostatic potential although the ultracapacitor, $\Phi(z)$, in turn, can be obtained by numerical integration of the one-dimensional Poisson equation:[30, 31]

$$\Phi(z) = -\frac{1}{\varepsilon_0}\int_{-z_0}^{z}(z - z')\,\rho_z(z')dz'$$

where $\rho_z(z')$ is the local charge density due to the atomic charge distribution of each ionic species. This distribution is given by:

$$\overline{\rho}(z) = \frac{1}{A}\int_{-x_0}^{x_0}\int_{-y_0}^{y_0} dx'dy'\rho_\alpha(x', y', z)$$

where A is the total surface area of the electrodes.

Figure 4 shows the electrostatic potential profiles for the PYR-TFSI ultracapacitor as a function of the charge density at the electrodes. For the other electrolytes, the curves are similar and presented in the supporting material. From these curves, we can obtain the potential drop, $\Delta\Phi$ through the device, in particular the zero charge potential, $\Delta\Phi^{descharg}$, is obtained for $\sigma = 0$ and is close to zero for the four electrolytes investigated here (ranging from 0.00 to 0.03 V) which is consistent with previously determined values computationally.[19, 32, 33] For all curves the oscillations of the electrostatic potential occur within only 2.5 nm, going to zero at higher distances. As expected, it was observed a gradual increase of the potential difference near the electrodes as the charge density is increased. This behavior is shown in Figure 5a.

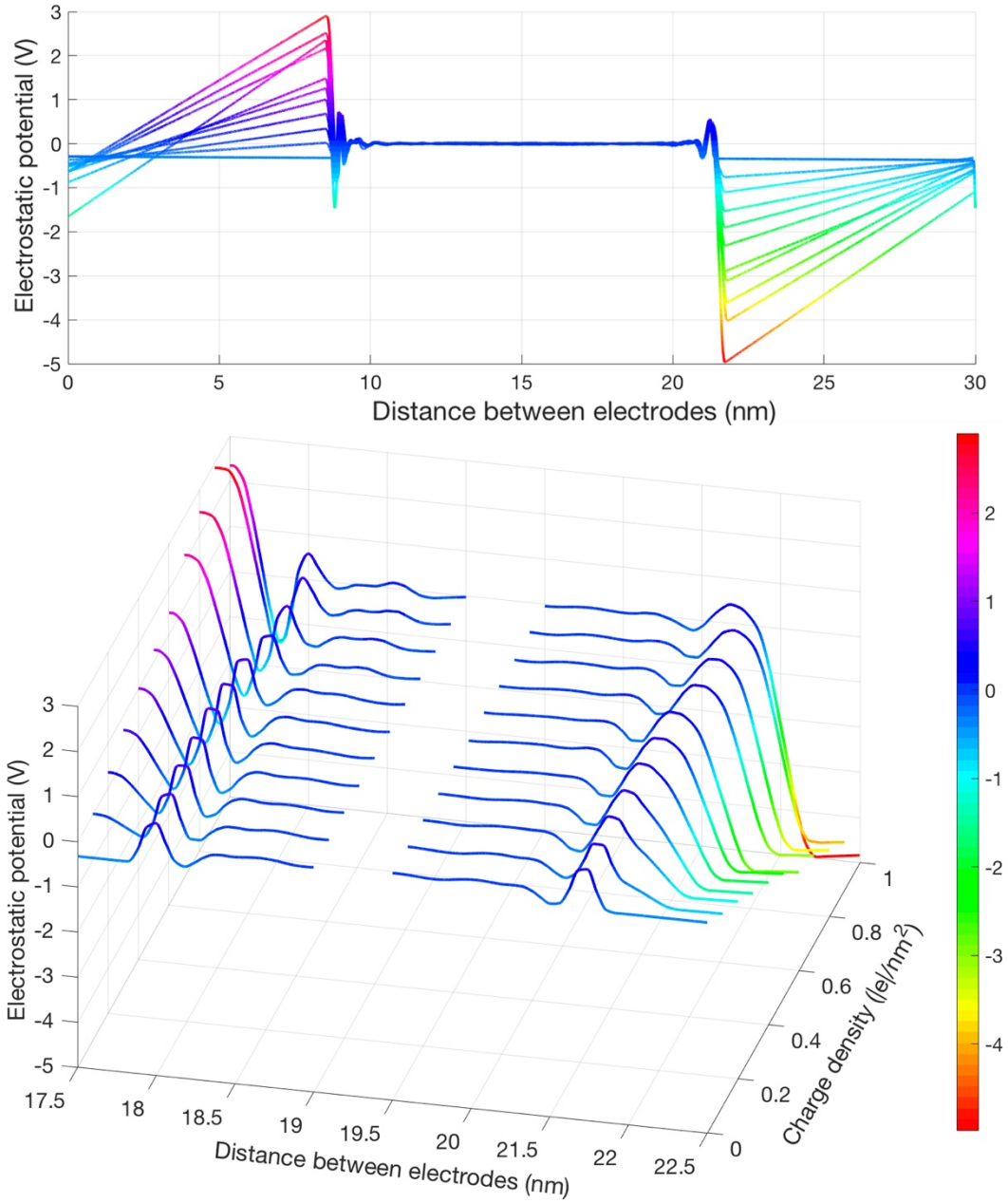

Figure 4: (Top) Electrostatic potential profile (V) for the PYR-TFSI ultracapacitor as a function of the distance (nm) from the electrodes and the surface charge density (nm^{-2}). At the top, the superimposed profiles are presented for all charge densities over the entire length of the simulation box, from 0 to 30 nm. (Bottom) is highlighted the potential near the positive electrode, in an enlarged scale and in perspective, to favored a comparison between the profiles. Numerical values for $\Delta\Phi$ are tabulated in the supporting material.

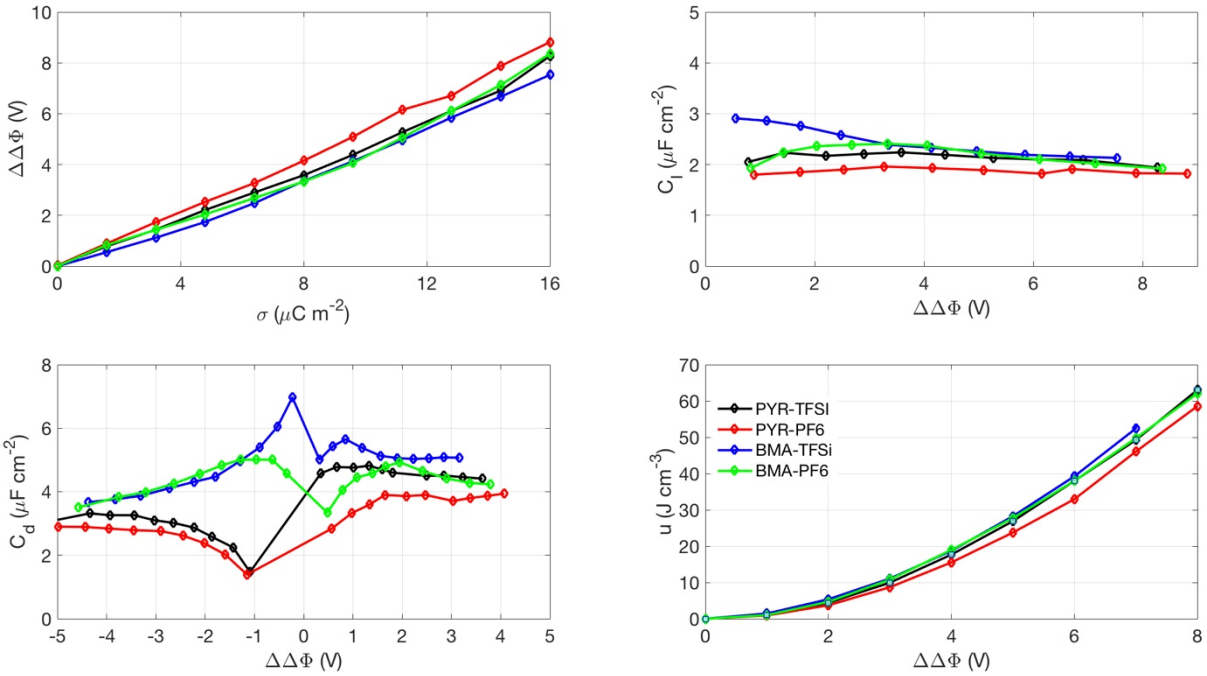

Figure 5: Electrical properties of ultracapacitors. a) variation of the electrostatic potential drop as a function of the charge density. b) integral capacitance as a function of the potential drop. c) differential capacitance as a function of the potential drop. d) energy density stored in the ultracapacitor as a function of the potential drop. Numerical values for ΔΦ are tabulated in the supporting material. An estimate for the error in each plot was made by dividing the trajectory into six different smaller blocks, calculating the properties and taking their standard deviation. For the sake of clarity these bars are not shown in the graph but are less than 8% for potential and capacitances and less than 14% for energy density.

Integral and differential capacitances as a function of the electrostatic potential are shown in Figures 5b and 5c. While the former is practically constant throughout the range of electrostatic potential, the latter present the typical variations observed ionic liquid electrolytes.[11, 32, 34, 35] Namely, it is known that the differential capacitance curves for ionic liquids can be of two types, camel or bell forms, being the first of two peaks and the second of a single peak. Due to the effects of the high temperature used in the simulations, the curve for capacitance difference presents wider and less pronounced peaks than the typical standard obtained experimentally. In spite of this, it is possible to clearly observe the camel behavior for the four ionic liquids, which is in agreement with several previous computational and experimental works.[11, 32, 34, 35]

The values for the capacitances obtained here are comparable to those found previously. For example, Guang and co-workers[36] determined the differential capacitance for a series of amino acids-based ionic liquids. They found that the capacitance of the ultracapacitors ranged from 3.9μF cm^{-2} to 5.9μF cm^{-2} at a potential difference of 2.2V. The authors seem to have observed no correlation between the capacitance values and the size of two ions used in electrolytes. Shim et.al.[29, 37] investigated a ultracapacitor whose electrolyte was a mixture of EMIM-BF4 and acetonitrile. The values reported were 3.6μF cm^{-2}. In the same work the pure liquid presented values slightly larger, 5.0-5.8μF cm^{-2}, depending on the temperature. Bedrov et al.[28] showed that the capacitance of the PYR13-FSI electrolyte, a similar liquid to PYR-TFSI used here, is about ~4.5 μF cm^{-2} at a potential of 2V. It has been observed that the experimental values for the capacitance are much higher than those obtained computationally.[28] However, this is not due to fundamental differences between the nature of the devices under comparison and the fact that in both computational and experimental practices different normalization factors are employed. In spite of this, experimental values found for differential specific capacitance compare well with the simulated counterparts, which in turn are compatible with the values reported here.[28]

The storage energy density in the ultracapacitor can be obtained from the relation between the values of the potential difference and the capacitance of the device, expressed by: $u = C_I[\Delta\Delta\Phi]^2/2V$, where V is the volume of the ultracapacitor (3.44x3.40x13.0=152.6nm^3). This relationship can be safely employed since it has been observed that the integral capacitance is constant over the entire range of potential difference. From Figure 5d we see that the energy density stored in the four ultracapacitors, as expected, increases quadratically with the potential across the device, being zero for the capacitor discharged and around 30 J cm^{-3} at a potential difference of 5.5 V. It is important to note that for an appropriate comparison the performance of the ultracapacitors in terms of stored energy was always taken to the same potential. Table 3 gives the values for the energy density of each ultracapacitor taken at the same potential

difference by interpolating the data from curves of Figure 5d. For example, for the potential of 5V, which is a threshold value reached in experiments with electrolytes based on ionic liquids, we observe energy density in a range of 24 to 28 J cm^{-3}.

Table 3. Stored energy density in each ultracapacitor, *u*, (J cm^{-3}) compared at several potential differences ΔΔΦ, (V).

	Stored energy density, *u*, (J cm^{-3})			
ΔΔΦ (V)	**PYR-TFSI**	**PYR-PF6**	**BMA-TFSI**	**BMA-PF6**
1.0	1.1	0.9	1.4	1.0
2.0	4.4	3.7	5.4	4.7
3.0	9.9	8.7	11.1	10.8
4.0	17.7	15.2	18.7	19.0
5.0	26.9	23.7	28.2	27.7
6.0	38.0	32.9	39.2	38.0
7.0	49.2	46.1	52.4	49.7
8.0	63.0	58.6	--	62.1

For potential differences, ΔΔΦ, ranging from 1.0 to 8.0 V, the average value of the integral capacitance varies from 1.9 μF cm^{-2} to 2.5 μF cm^{-2} which corresponds to the liquids PYR-PF6 and BMA-TFSI, respectively. We also note that although the performance difference between all liquids is not large, these liquids consistently present the highest and lowest performances among the four evaluated. However, PYR-PF6 and BMA-TFSI do not present extreme volumes (maximum or minimum) (see Table 4), so no correlation between ion pair volume and performance can be established. A stronger indicator for this set of ultracapacitors seems to be the ratio R between the volumes of the ions constituting the electrolyte. We see that for the liquid PYR-PF6, which presents the lowest performance this ratio is maximum; the cation being 2.5 times larger than the anion. On the other hand, for the BMA-TFSI liquid, whose performance is the largest, R = 1, with anion and cation having virtually the same size.

Table 4. Integral capacitance average, $\langle C_I \rangle$, (μF cm^{-2}), molar mass, M, (g mol^{-1}); molar volume, V_S, (cm^3 mol^{-1}) obtained by dividing the volume of the simulation cell of the pure liquid by the number of ionic pairs; molar volume, V_Q, (cm^3 mol^{-1}) obtained by quantum calculations. In brackets the volume values of cations and ions are shown separately. The molar volume was determined using the program Gaussian 09[38] optimizing the ion pair at theoretical level B3LYP/6-311+(d, p).

	PYR-TFSI	**PYR-PF6**	**BMA-TFSI**	**BMA-PF6**
$\langle C_I \rangle$	2.1	1.9	2.5	2.2
M	423	287	396	261
V_S	348	276	326	255
V_Q	[135]+[113]=248	[135]+[54]=189	[111]+[113]=224	[111]+[54]=165
R	1.2	2.5	1.0	2.1

Here two important observations are noteworthy. First, capacitance originates from a balance of ion-ion-electrode attraction/repulsion, i.e. it is determined by distribution of atomic charges in the near-electrode space. Small ions could have seemingly formed a thin charged layer, which would result in a high capacitance, but they repel strongly from one another because its atomic charges are large and not buried. Therefore, our initial expectation that the lower ions of the ionic liquids would imply better capacitance was not observed. Second, the correlation with the R factor presented here should not be generalized since it was observed only for this small set of investigated ionic liquids. Additional investigations, both computational and experimental, would be crucial for elucidating these two aspects.

CONCLUSIONS

The performance of four different ionic liquid based electrolytes was compared through atomistic molecular dynamics simulation results. The liquids formed by two different types of cations and two different types of anions were chosen in order to provide a margin for direct comparison between their properties. Our structural analysis confirms that in all cases the structure of the electric double layer depends strongly on the charge density on the electrodes. This structuring of the ionic liquid is corroborated by the analysis of the electrolyte-

electrode interactions in the ultracapacitor, which indicates that such interactions are predominantly of the van der Waals type for all cases. The electrostatic contribution becomes significant, > 10% van der Waals, only at charge densities higher than 0.4*e* nm^{-2}.

For the set of ionic liquids investigates here, any correlation for the ultracapacitor properties with the ion pair volume (and indirectly the molar mass) could be made. However, we observed that the ratio R between the volumes of the ions constituting the electrolyte can be associated with the EDL capacitance and roughly with its performance. In this case, we found that for the liquid that presents the lowest capacitance (PYR-PF6) the R ratio is maximum; i.e. the cation is 2.5 times larger than the anion. On the other hand, for the BMA-TFSI liquid, whose performance is the largest, R = 1, with anion and cation having virtually the same size. In general, we observed that the electrolytes formed by ions of similar volumes show better performance, however a definitive correlation between the ionic size ratio and the performance of supercapacitors cannot be made in this study. Additional investigations are desirable, from both computational and experimental approaches, to ensure this tendency.

ACKNOWLEDGMENTS

E.E.F gratefully acknowledges support from FAPESP (São Paulo Research Foundation, Grant Number 2017/11631-2), Shell, the strategic importance of the support given by ANP (Brazil's National Oil, Natural Gas and Biofuels Agency) through the R&D levy regulation and CNPq (National Council for Scientific and Technological Development). E.E.F also is particularly grateful for the contribution given by Dr. Marcos Quiles.

CONTACT INFORMATION

Any correspondence concerning this work can be forwarded to fileti@gmail.com (E.E.F) or vvchaban@gmail.com (V.V.C) or nadezhda.a.andreeva@gmail.com (N.A.A).

REFERENCES

1. R. Burt, G. Birkett and X. S. Zhao, *Physical Chemistry Chemical Physics*, 2014, **16**, 6519-6538.

2. Z. Yu, L. Tetard, L. Zhai and J. Thomas, *Energy & Environmental Science*, 2014, **8**, 702-730.

3. E. Frackowiak, Q. Abbas and F. Béguin, *Journal of Energy Chemistry*, 2013, **22**, 226-240.

4. L. Zhang, R. Zhou and X. S. Zhao, *Journal of Materials Chemistry*, 2010, **20**, 5983-5992.

5. L. Xia, L. Yu, D. Hu and G. Z. Chen, *Materials Chemistry Frontiers*, 2017, **1**, 584-618.

6. A. S. Shaplov, R. Marcilla and D. Mecerreyes, *Electrochimica Acta*, 2015, **175**, 18-34.

7. A. J. R. Rennie, N. d. Sanchez-Ramirez, R. M. Torresi and P. J. Hall, *The Journal of Physical Chemistry Letters*, 2013, **4**, 2970-2974.

8. J. Vatamanu, Z. Hu, D. Bedrov, C. Perez and Y. Gogotsi, *The Journal of Physical Chemistry Letters*, 2013, **4**, 2829-2837.

9. M. Wu, W. Li, S. Li and G. Feng, *RSC Advances*, 2017, **7**, 28945-28950.

10. J. Vatamanu, O. Borodin, D. Bedrov and G. D. Smith, *J. Phys. Chem. C*, 2012, **116**, 7940–7951.

11. D. Bedrov, J. Vatamanu and Z. Hu, *Journal of Non-Crystalline Solids*, 2015, **407**, 339-348.

12. G. Bussi, D. Donadio and M. Parrinello, *Journal of Chemical Physics*, 2007, **126**, 014101.

13. V. V. Chaban, E. E. Fileti and O. V. Prezhdo, *J. Phys. Chem. C*, 2017, **121**, 911–917.

14. V. V. Chaban and E. E. Fileti, *RSC Advances*, 2015, **5**, 81229-81234

15. I. V. Voroshylova and V. V. Chaban, *J. Phys. Chem. B*, 2014, **118**, 10716-10724.

16. V. V. Chaban and I. V. Voroshylova, *J. Phys. Chem. B*, 2015, **119**, 6242-6249.

17. J. N. C. Lopes, J. Deschamps and A. A. H. Padua, *J. Phys. Chem. B*, 2004, **108**, 2038-2047.

18. S. Zhang, Z. Bo, H. Yang, J. Yang, L. Duan, J. Yan and K. Cen, *Journal of Power Sources*, 2016, **334**, 162-169.

19. H. Yang, X. Zhang, J. Yang, Z. Bo, M. Hu, J. Yan and K. Cen, *The Journal of Physical Chemistry Letters*, 2016, DOI: 10.1021/acs.jpclett.6b02659.

20. E. Paek, A. J. Pak, K. E. Kweon and G. S. Hwang, *The Journal of Physical Chemistry C*, 2013, **117**, 5610-5616.

21. E. Paek, A. J. Pak and G. S. Hwang, *The Journal of Physical Chemistry C*, 2013, **117**, 23539-23546.

22. E. Lindahl, B. Hess and D. Van Der Spoel, *Journal of Molecular Modeling*, 2001, **7**, 306-317.

23. H. J. C. Berendsen, D. Vanderspoel and R. Vandrunen, *Computer Physics Communications*, 1995, **91**, 43-56.

24. M. Kunze, M. Montanino, G. B. Appetecchi, S. Jeong, M. Schonhoff, M. Winter and S. Passerini, *J Phys Chem A*, 2010, **114**, 1776-1782.

25. A. Deyko, K. R. J. Lovelock, J. A. Corfield, A. W. Taylor, P. N. Gooden, I. J. Villar-Garcia, P. Licence, R. G. Jones, V. G. Krasovskiy, E. A. Chernikovab and L. M. Kustov, *Phys. Chem. Chem. Phys.*, 2009, **11**, 8544–8555.

26. S. Zhang, X. Lu, Q. Zhou, X. Li, X. Zhang and S. Li, *Ionic Liquids. Physicochemical properties*, Elsevier, Oxford, 2009.

27. S.-W. Park, A. D. DeYoung, N. R. Dhumal, Y. Shim, H. J. Kim and Y. Jung, *The Journal of Physical Chemistry Letters*, 2016, **7**, 1180-1186.

28. J. Vatamanu, L. Xing, W. Li and D. Bedrov, *Physical Chemistry Chemical Physics*, 2014, **16**, 5174-5182.

29. Y. Shim, H. J. Kim and Y. Jung, *Faraday Discussions*, 2011, **154**, 249-263.

30. S. A. Kislenko, I. S. Samoylova and R. H. Amirova, *Physical Chemistry Chemical Physics*, 2009, **11**, 5584–5590.

31. Z. Wang, D. L. Olmsted, M. Asta and B. B. Laird, *Journal of Physics: Condensed Matter*, 2016, **28**, 464006.

32. X. Liu, Y. Wang, S. Li and T. Yan, *Electrochimica Acta*, 2015, **184**, 164-170.

33. G. Feng, J. S. Zhang and R. Qiao, *The Journal of Physical Chemistry C*, 2009, **113**, 4549-4559.

34. J. B. Haskins and J. W. Lawson, *The Journal of Chemical Physics*, 2016, **144**, 184707.

35. S. Li, G. Feng and P. T. Cummings, *Journal of Physics: Condensed Matter*, 2014, **26**, 284106.

36. M. Wu, W. Li, S. Li and G. Feng, *RSC Advances*, 2017, **7**, 28945-28950.

37. Y. Shim, Y. Jung and H. J. Kim, *The Journal of Physical Chemistry C*, 2011, **115**, 23574-23583.

38. M. J. Frish and e. al., *Journal*, 2009.